
This is an electronic reprint of the original article.
This reprint may differ from the original in pagination and typographic detail.

Miao, Ziyue; Tan, Hongwei; Gustavsson, Lotta; Zhou, Yang; Xu, Quan; Ikkala, Olli; Peng, Bo
Gustation-Inspired Dual-Responsive Hydrogels for Taste Sensing Enabled by Machine Learning

Published in:
Small

DOI:
[10.1002/smll.202305195](https://doi.org/10.1002/smll.202305195)

Published: 15/02/2024

Document Version
Publisher's PDF, also known as Version of record

Published under the following license:
CC BY

Please cite the original version:
Miao, Z., Tan, H., Gustavsson, L., Zhou, Y., Xu, Q., Ikkala, O., & Peng, B. (2024). Gustation-Inspired Dual-Responsive Hydrogels for Taste Sensing Enabled by Machine Learning. *Small*, 20(7), Article 2305195. <https://doi.org/10.1002/smll.202305195>

This material is protected by copyright and other intellectual property rights, and duplication or sale of all or part of any of the repository collections is not permitted, except that material may be duplicated by you for your research use or educational purposes in electronic or print form. You must obtain permission for any other use. Electronic or print copies may not be offered, whether for sale or otherwise to anyone who is not an authorised user.

Gustation-Inspired Dual-Responsive Hydrogels for Taste Sensing Enabled by Machine Learning

Ziyue Miao, Hongwei Tan, Lotta Gustavsson, Yang Zhou, Quan Xu, Olli Ikkala,* and Bo Peng*

Human gustatory system recognizes salty/sour or sweet tastants based on their different ionic or nonionic natures using two different signaling pathways. This suggests that evolution has selected this detection dualism favorably. Analogically, this work constructs herein bioinspired stimulus-responsive hydrogels to recognize model salty/sour or sweet tastes based on two different responses, that is, electrical and volumetric responsivities. Different compositions of zwitter-ionic sulfobetainic *N*-(3-sulfopropyl)-*N*-(methacryloxyethyl)-*N,N*-dimethylammonium betaine (DMAPS) and nonionic 2-hydroxyethyl methacrylate (HEMA) are co-polymerized to explore conditions for gelation. The hydrogel responses upon adding model tastant molecules are explored using electrical and visual de-swelling observations. Beyond challenging electrochemical impedance spectroscopy measurements, naive multimeter electrical characterizations are performed, toward facile applicability. Ionic model molecules, for example, sodium chloride and acetic acid, interact electrostatically with DMAPS groups, whereas nonionic molecules, for example, D(-)fructose, interact by hydrogen bonding with HEMA. The model tastants induce complex combinations of electrical and volumetric responses, which are then introduced as inputs for machine learning algorithms. The fidelity of such a trained dual response approach is tested for a more general taste identification. This work envisages that the facile dual electric/volumetric hydrogel responses combined with machine learning proposes a generic bioinspired avenue for future bionic designs of artificial taste recognition, amply needed in applications.

1. Introduction

Tongue is a soft and sensitive gustatory organ, secreting taste buds with protein receptors and ion channels.^[1] In mammals, five primary tastes, that is, sweetness, sourness, saltiness, bitterness, and umami are distinguished by the gustatory system.^[2] Among them, sweetness, bitterness, and umami are perceived by binding the water-soluble nonionic tastant molecules to G-protein-coupled receptors in the taste buds,^[3,4] whereas the other tastes are triggered by the reception of hydrogen ions^[5] and alkali metallic^[6] (mainly sodium) ions within ion channels.^[7] In particular, sensing of sweetness, saltiness, and sourness is of technological relevance because they are associated with nutritional values and correspond to the palatability of food and beverage at weak and medium concentrations but should be avoided at strong concentrations.^[8]


Designing artificial taste sensors has so far been approached predominantly based on complex electrical detection based on potentiometry and voltammetry by using engineered membranes and electrodes.^[9,10] Therein, a large amount

of electric data is required and analyzed with sophisticated algorithms. On the other hand, different hydrogels can be considered as synthetic representatives of biological soft tissues.^[11,12] As hydrogels allow different functionalizations for various stimuli-responses, it is natural to consider whether hydrogels could allow bioinspired taste sensing, suggested by tongues.^[13,14] Indeed, recent progress has shown either specific taste recognition for a single tastant^[15,16] or specific differentiation between bitterness and astringency^[13] by copolymeric hydrogels based on electrical signals. However, allowing recognition of multiple tastes with reasonable selectivity and sensitivity using solely electronic detection of hydrogel is challenging.^[13] By contrast, one could ask whether the biological concept to recognize a wide range of tastes using two different mechanisms could suggest constructing hydrogels also with another response beyond the electrical signal. Therein, a natural choice for the additional response beyond the electrical response could be the swelling/deswelling of hydrogels, which has been explored extensively for other stimuli.^[17,18]

Z. Miao, H. Tan, L. Gustavsson, O. Ikkala, B. Peng
Department of Applied Physics
Aalto University
Aalto FI-00076, Finland
E-mail: olli.ikkala@aalto.fi; bo.peng@aalto.fi; peng_bo@fudan.edu.cn

Z. Miao, B. Peng
Department of Materials Science
Fudan University
Shanghai 200433, China

Y. Zhou, Q. Xu
State Key Laboratory of Heavy Oil Processing
China University of Petroleum (Beijing)
Beijing 102249, China

 The ORCID identification number(s) for the author(s) of this article can be found under <https://doi.org/10.1002/smll.202305195>

© 2023 The Authors. Small published by Wiley-VCH GmbH. This is an open access article under the terms of the Creative Commons Attribution License, which permits use, distribution and reproduction in any medium, provided the original work is properly cited.

DOI: 10.1002/smll.202305195

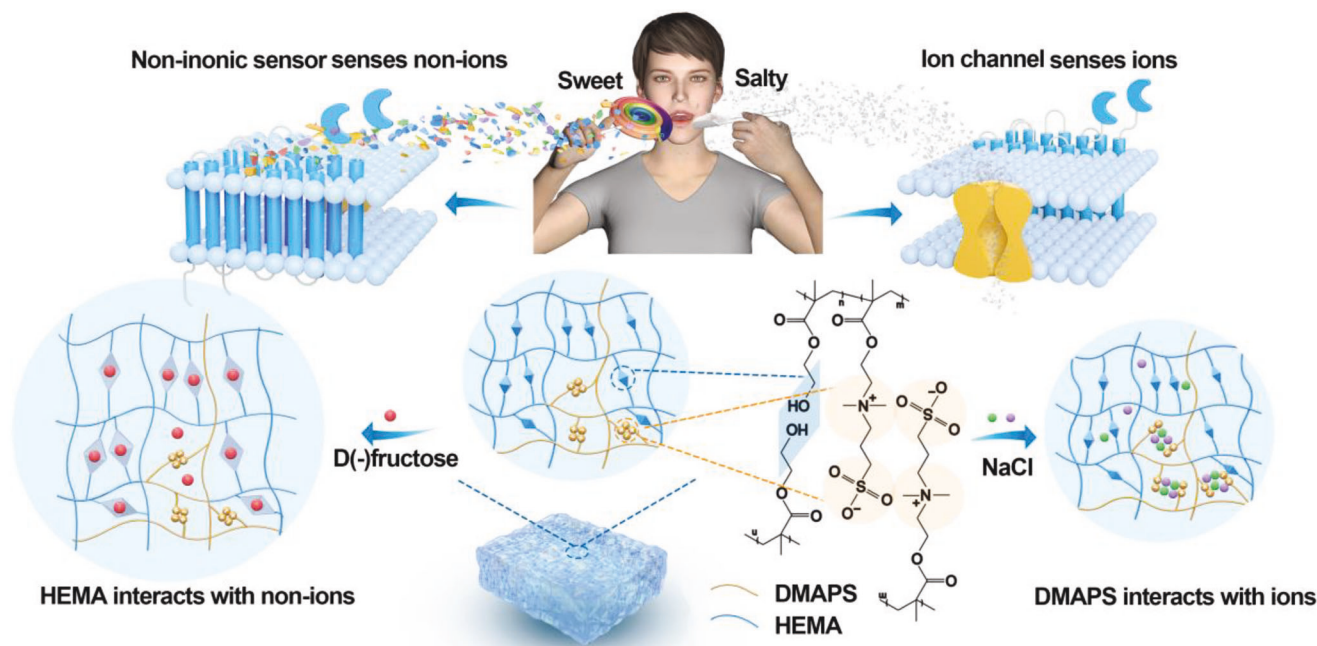


Figure 1. Schematic illustration of biological gustation sensing and a bioinspired hydrogel dual-responsive sensor poly(DMAPS-co-HEMA), involving both electrical and volumetric responses.

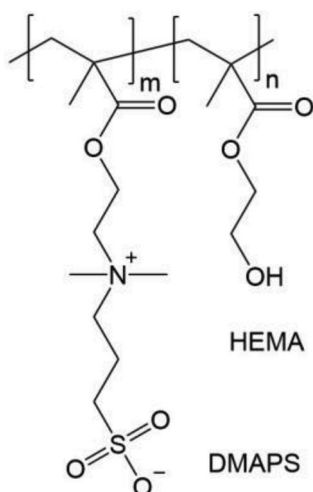
Therefore, inspired by gustatory principles, we propose a bionic design of a copolymeric hydrogel with zwitter-ionic and nonionic functional groups that enable the sensation of sweetness, saltiness, and sourness by two responses, that is, by electrical and volumetric changes (Figure 1). The hydrogel is synthesized by co-polymerizing nonionic monomer 2-hydroxyethyl methacrylate (HEMA) and zwitter-ionic monomer *N*-(3-sulfopropyl)-*N*-(methacryloxyethyl)-*N,N*-dimethylammonium betaine (DMAPS), see Scheme 1. Anal-

gous to protein receptors and ion channels in gustatory systems, the HEMA units aim to interact with nonionic tastants, (e.g., sugar), while DMAPS associates with ionic tastants (e.g., NaCl and acids). Density functional theory (DFT) simulations unravel the molecular interactions. By having two input variables, that is, the electrical and volumetric ones, enhances the feasible identification of multi-/mixed tastes using machine learning.

2. Results and Discussion

2.1. Hydrogels and Their Characterization

We will first present the polymerization and characterization of poly(DMAPS-co-HEMA). Poly(HEMA) is extensively used in bio-related applications due to its biocompatibility.^[19,20] It has also been employed to promote water dispersibility of poorly water-soluble drugs due to its interactions.^[21,22] Herein, we expected HEMA to interact with nonionic tastants via hydrogen bonds.^[23,24] On the other hand, zwitter-ionic polymers, such as poly(DMAPS) are known to interact with ions.^[25,26] Therefore, we expected these two comonomers to allow different bindings for ionic and nonionic additives and therefore different stimulus responses. Herein, the polymerization is made using free radical polymerization in water using their different mole fractions from 75:25, 80:20, 86:14, 89:11, 91:0 to 100:0 mol:mol (for details see Experimental Section). To allow gelation, the presence of the HEMA component is needed as seen in Figure 2a for a ternary phase diagram, also depicting the minimum solid aq. concentration to allow gelation at different poly(DMAPS-co-HEMA) compositions. Although the gelation takes place at the minimum solid aq. concentration < 30 wt%, for the sake of easy implementation in the tastant detection, that is, to retain gelation during



Scheme 1. Poly(HEMA-co-DMAPS) constructed with nonionic monomer 2-hydroxyethyl methacrylate (HEMA) and zwitter-ionic monomer *N*-(3-sulfopropyl)-*N*-(methacryloxyethyl)-*N,N*-dimethylammonium betaine (DMAPS).

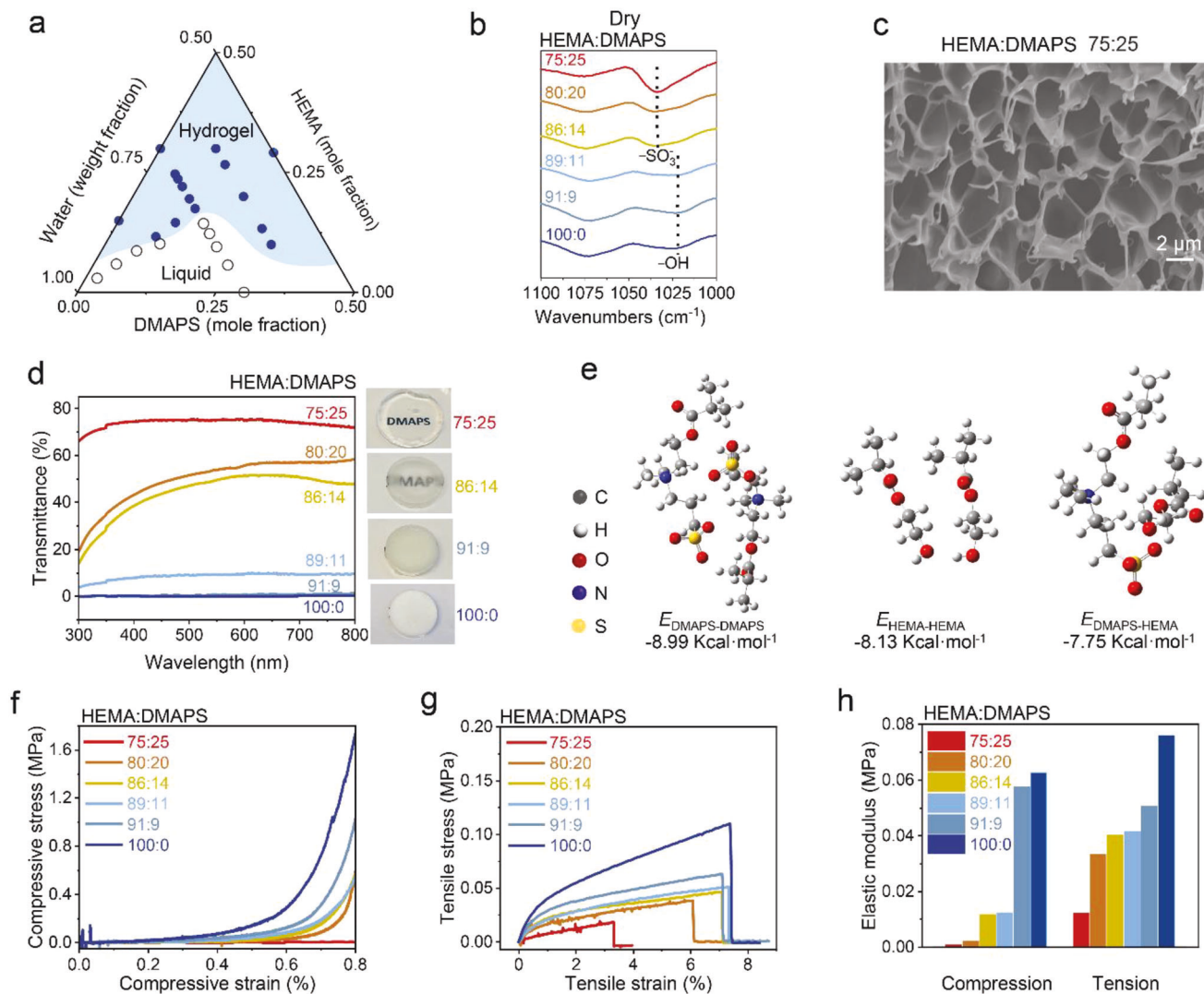


Figure 2. Characterization of poly(DMAPS-*co*-HEMA) hydrogels. a) Poly(DMAPS-*co*-HEMA)/water ternary phase diagram illustrating the compositions leading to hydrogelation. b) magnified FTIR spectra of poly(DMAPS-*co*-HEMA) upon drying. c) A representative scanning electron microscopy image of poly(DMAPS-*co*-HEMA) (75:25 mol:mol) freeze-dried with liquid propane and cross-sectionally cut by a focused ion beam. d) UV-vis transmission spectra of hydrogels. e) Density functional theory optimized interactions of DMAPS-DMAPS, HEMA-HEMA and DMAPS-HEMA molecules. f–h) Compressive stress-strain curves, tensile stress-strain curves, and elastic moduli of hydrogels at different compositions of poly(DMAPS-*co*-HEMA).

the immersion in tastant solution, 30 wt% of copolymers in water was selected in the following experiments.

To explore the physicochemical properties, we first vary the molar ratio of HEMA versus DMAPS. In Fourier-transform infrared spectroscopy (FTIR) spectra of dried poly(DMAPS-*co*-HEMA), the pattern intensity of the sulfonate group at 1043 cm^{-1} decreases by reducing the DMAPS molar fraction while the peak at 1023 cm^{-1} assigned to the hydroxyl groups of HEMA increases, as shown in Figure 2b and Figure S1, Supporting Information. The chemical composition of HEMA and DMAPS in the hydrogels is also verified by solid-state nuclear magnetic resonance spectroscopy (Figure S2, Supporting Information). Upon freeze-drying from liquid propane, the hydrogels show interconnected porous structure with an average pore size of $3.1\text{ }\mu\text{m}$ and wall thickness of $0.36\text{ }\mu\text{m}$ for HEMA:DMAPS at 75:25 mol:mol

(Figure 2c and Figure S3, Supporting Information). These length scales facilitate broadband visible light scattering.^[27,28]

Increasing the amount of HEMA leads to opaque hydrogel (see Figure 2d), which is due to the phase separation of the less hydrophilic HEMA units in water.^[29] Quantitatively, the transmittance of 5 mm-thick hydrogels in the wavelength range of 300–800 nm is totally suppressed as the molar concentration of HEMA is increased up to 91% (Figure 2d). The intermolecular interactions studied by DFT reveal the in-depth reason: the HEMA units are prone to interact with the other HEMA units instead of with water (Figure S4, Supporting Information), thus leading to aggregation. By contrast, DMAPS favors attraction to water (Figure S5, Supporting Information), which increases the optical transparency. Figure 2e shows that the binding energies of DMAPS-DMAPS and HEMA-HEMA are higher than

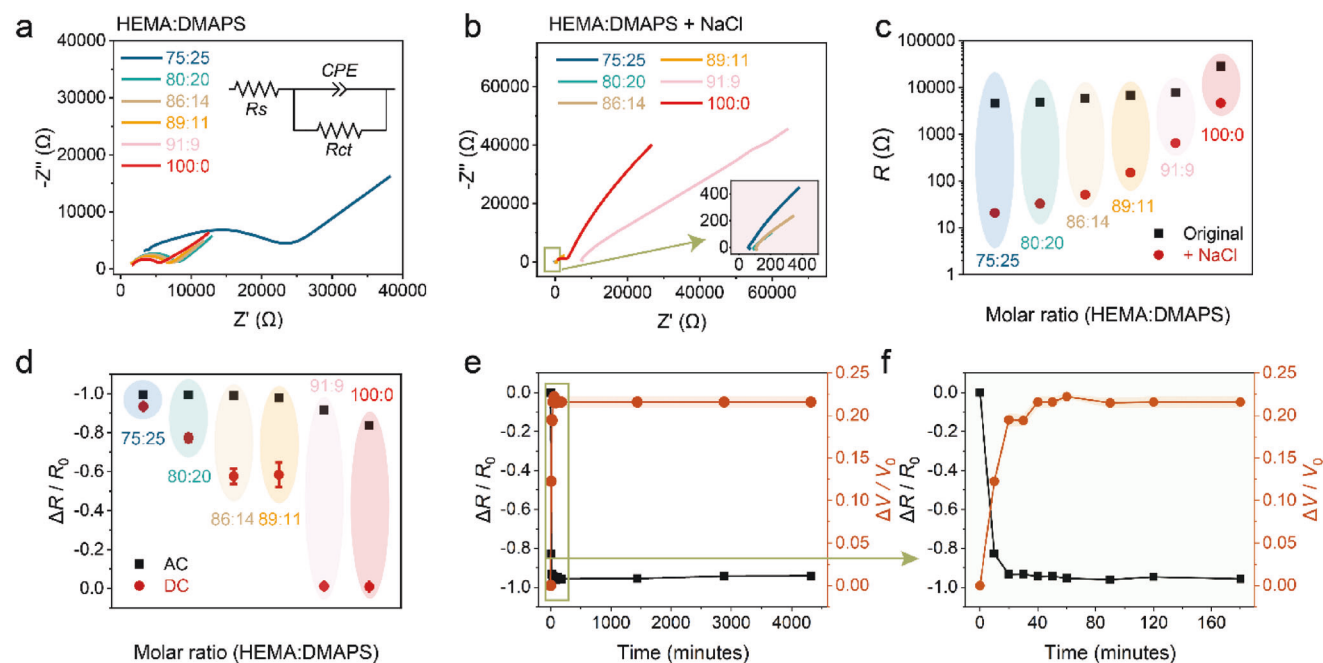


Figure 3. Electrical and volumetric properties of poly(DMAPS-*co*-HEMA) hydrogels. a) Electrochemical impedance spectra of hydrogels made by different molar ratio of HEMA/DMAPS (the inset is the equivalent circuit). b) Impedance spectra of hydrogels after immersion in NaCl solutions (0.17 M). c) Total bulk resistance comparison of hydrogels with or without NaCl, calculated from the impedance data. d) The relative resistance-changes of hydrogels with NaCl measured by AC and DC fields at a voltage of 1 V. e,f) Dynamic resistance and volumetric response of hydrogels to NaCl solution, measured with the DC field. Sample size $n = 3$ in d–f); error bars correspond to standard deviation, SD.

that of DMAPS-HEMA, indicating that there might be micro-phase separation among hydrogels.

Notably, the poly(DMAPS-*co*-HEMA) composition grossly affects the mechanical properties. In compression (Figure 2f), all compositions show a linear region of elastic deformation at strains up to $\approx 40\%$, with a rapid increase of stress at higher strains due to densification.^[30,31] The compressive elastic modulus increases for higher mole fraction of HEMA, which is also observed in tensile measurements (Figure 2g,h).

2.2. Electrical and Volumetric Gustatory Responses

Next, we investigate the electrical performance of poly(DMAPS-*co*-HEMA) hydrogels in response to different tastant molecules. For an initial exploration, the hydrogels with different DMAPS contents are immersed into NaCl 0.17 M aqueous solutions over 24 h to reach equilibrium. Electrical impedance spectroscopy is applied to reveal the ionic transport (Figure 3a,b). At high frequencies, the intercept of the semicircle at X-axis denotes the equivalent series resistance (R_s), and the diameter of semicircle represents the charge transfer resistance (R_{ct}) between the electrolyte and the electrode. However, at relatively low frequencies, the non-vertical line is defined as the diffuse layer resistance. In the equivalent circuit diagram acquired from Nyquist data, the values of R_s , R_{ct} and a constant phase element CPE (accounts for inhomogeneous or imperfect capacitance)^[32] can be found. Here, R_{ct} is chosen as the total bulk resistance of hydrogels. In comparison to pristine poly(DMAPS-*co*-HEMA) hydrogels, their electrical resistance decreases after immersion in a salt solution. As a

larger fraction of DMAPS is copolymerized in the hydrogel network, the resistance becomes pronounced (Figure 3c), indicating the vital role of DMAPS in accommodating ions. This “salt-in” effect is due to the anti-polyelectrolyte effect,^[33] where DMAPS is capable of binding ions through its cationic ammonium and anionic sulfonate groups. Pure poly(HEMA) hydrogels have a low conductivity with only a marginal effect on resistance upon immersing in a NaCl solution. Thus, poly(HEMA) hydrogel is considered insensitive to NaCl.^[34]

Although electrochemical impedance spectroscopy allows in-depth electrical characterization, it is fundamentally a complex measurement setup. A quest exists, whether even simplistic voltmeters using direct current (DC) measurement could be used, allowing as a facile sensing for practical applications. As shown in Figure 3d, the electrical resistance results of hydrogels measured using alternating current (AC) and DC (at a voltage of 1 V) fields have been compared. In both cases, the relative resistance-changes of hydrogels immersed in NaCl (0.17 M) decrease as increasing the ratio between HEMA and DMAPS. Whereas, it shows that in poly(DMAPS-*co*-HEMA) at 75:25 mol:mol using NaCl (0.17 M) the two methods seem to qualitatively match. For the sake of easy implementation and analysis subject to matching between DC and AC results, the DC field is used exclusively for hydrogels with a HEMA/DMAPS ratio of 75:25 mol:mol in the following experiments.

Beyond the electrical response, the salty NaCl tastant also affects the volume of poly(DMAPS-*co*-HEMA) hydrogels by deswelling (Figure 3e,f). Therefore, we simultaneously monitor the temporary variations of volume and resistance in hydrogels upon immersing them into the NaCl solution (0.17 M). Both

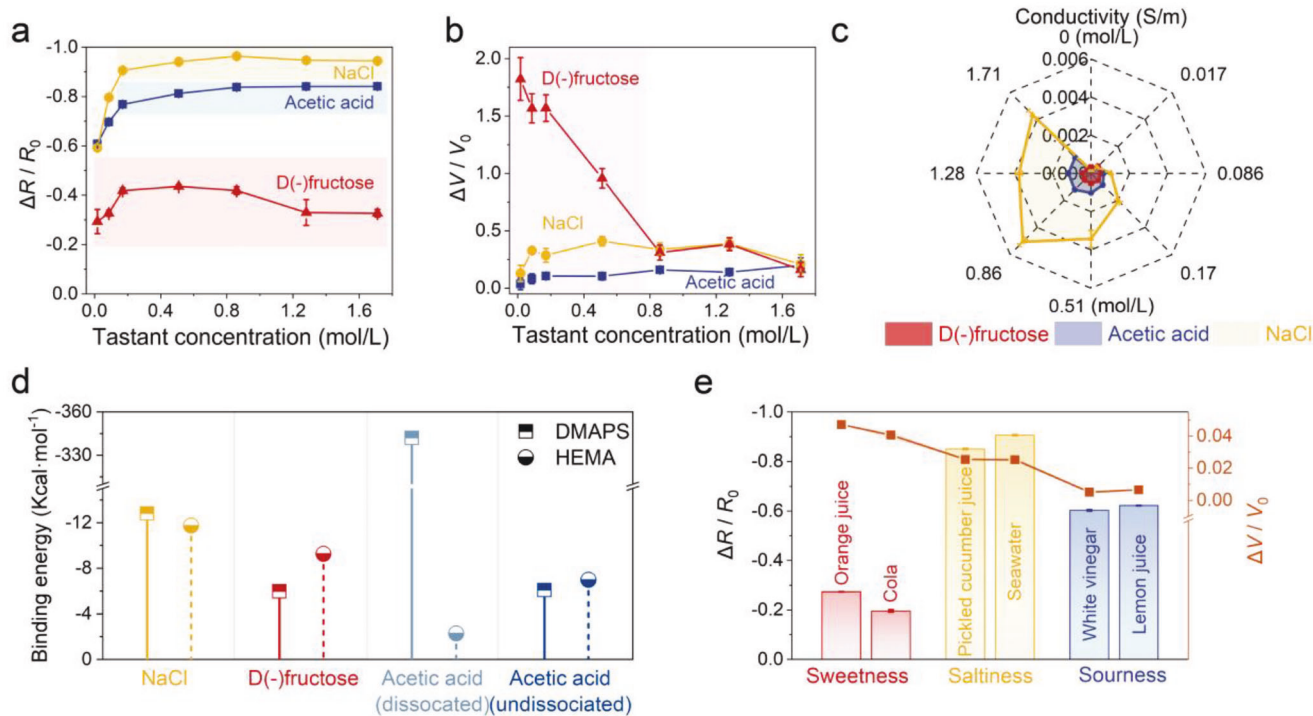


Figure 4. Tastant recognition. a–c) Relative resistance-change, relative volume-change, and conductivity of hydrogels in response to tastants of D(-)-fructose, NaCl, and acetic acid using DC fields of 1 V. d) Theoretical exploration of interactions between comonomers and tastants. e) Gustatory sensing of representative commercial beverages and foods (orange juice, cola, pickled cucumber juice, seawater, white vinegar, and lemon juice) with hydrogels. Sample size $n = 3$ in a–e); error bars correspond to SD.

resistance and volume changes are stabilized within 40 min of immersion (Figure 3f), and are equilibrated within 3 days. The variation after 1 day is very minor (<5%). To minimize this variation, we immersed the hydrogels overnight in solution. This response is slower in contrast to human taste response, that is, <1s.^[35] Rapid response can be achieved via size reduction of the sensor or the introduction of external stimuli to accelerate the tastant diffusion.^[36] Additionally, the stability of hydrogel sensors sealed in Petri dishes at ambient temperature was tested over 10 days (Figure S6a, Supporting Information). No significant change in the sensitivity of hydrogels in response to NaCl solution (0.17 M) was observed, indicating the durable stability of hydrogels in sensing tastants. Furthermore, the hydrogel exhibits nearly identical taste sensitivity at 5 °C, room temperature (RT), and 40 °C (Figure S6b, Supporting Information), affirming the temperature-independent stability of the hydrogel sensor.

Interestingly, the used poly(DMAPS-co-HEMA) hydrogels respond differently to weakly ionic acetic acid and nonionic tastants in contrast to the NaCl compounds. Therein, when the hydrogels are immersed with aqueous solutions of acetic acid or D(-)-fructose at different concentrations, the relative resistance-change $\Delta R/R_0$ increases as more tastants are used until reaching a plateau (Figure 4a). This is also observed for salt solutions. It seems there is a maximum capacity for hydrogel in accommodating tastant molecules. Among tastants, they are slightly different, that is, -0.6 for NaCl, -0.8 for acetic acid, and -0.3 for D(-)-fructose in relative resistance-change $\Delta R/R_0$. Correspondingly, the maximum capacity of tastants seems similar, that is, about 0.2 mol L⁻¹, possibly caused by the discrepancy between

HEMA and DMAPS in accommodating ionic and nonionic tastant molecules. Beyond these thresholds, the relative resistance-changes among tastants are distinct, facilitating the recognition of different tastes. Simultaneously, the volume changes are also monitored (Figure S7, Supporting Information). The relative volume-changes $\Delta V/V_0$ of hydrogels in D(-)-fructose solution is different from the other solutions (Figure 4b). In sweet solutions, the swelling of hydrogels drops as increasing the concentration of D(-)-fructose to its minimum at ≈ 0.86 M. In contrast, the sour and salty solutions make hydrogels less swollen with an order of sour > salty. These observations might be related to the interactions between polymer networks and tastants, which will be discussed later. Furthermore, the ionic conductivity of hydrogels (Figure 4c) is calculated based on the resistances and the volume of hydrogels (for details see the Experimental section). The conductivity of the hydrogel is independent to D(-)-fructose concentration, while a slight increase is observed with the addition of acetic acid, and it is highly correlated to the NaCl content.

To understand the responsiveness of the hydrogel, we applied DFT simulations to understand the interactions between polymer units and solutes. For the zwitter-ionic DMAPS units, anti-parallel dipolar alignment is suggested due to the electrostatic dipolar interactions (Figure 2f). The addition of NaCl drives these coupled zwitter-ionic groups to be dissociated, that is, the sulfonate and amino groups attract sodium cations and chlorine anions, respectively (Figure 4d and Figure S9, Supporting Information). This expands the zwitter-ions, causing volume expansion of the hydrogel and thus increasing the conductivity due to free ions. However, the zwitter-ionic polymer chains are

confined within the HEMA network, thus exhibiting a limited swelling response in volume to the NaCl tastant. In contrast, D(-)-fructose, a nonionic molecule, has little effect on the relative resistance change of the hydrogel. It shows a weaker attraction to DMAPS than to HEMA, inserting into HEMA network and significantly swelling the hydrogel (Figure 4d and Figure S7, Supporting Information). As to acetic acid, it is calculated to be attracted by DMAPS with a significant binding energy of $-341.95 \text{ kcal mol}^{-1}$ (Figure S9, Supporting Information). However, only 0.36% of acetic acid molecules are dissociated at the concentration of 0.83 M (20 °C), releasing $\approx 0.003 \text{ M}$ hydrogen ions^[37] (see Supporting Information). The non-ionized acetic acid in the hydrogel is the dominant form, showing a favorable affinity to HEMAS than to DMAPS, like D(-)-fructose (Figure 4d). The coexistence of non-ionized and ionized acetic acid in the hydrogels leads to resistance- and volume-changes between those of D(-)-fructose and NaCl (Figure S10, Supporting Information).

At large, D(-)-fructose, NaCl, and acetic acid represent three typical flavors: sweetness, saltiness, and sourness, respectively.^[38] Poly(DMAPS-co-HEMA) hydrogels enable the recognition of these three model tastants from the electrical response at a relatively high concentration of tastants, for example, $>0.2 \text{ M}$, while differentiate in terms of volume variation at low tastant concentrations $<0.8 \text{ M}$ (see the highlighted regions in Figure 4a,b). This behavior can be used in further developing a prototypical artificial tongue.

Although the electric conductivity of D(-)-fructose, NaCl, and acetic acid solutions (Figure S8a, Supporting Information) is discrepant, providing a possible way to discern them, machine learning requires a large amount of data for accurate discernment. The volumetric response data from hydrogel sensors offers additional data as the secondary set of the input for machine learning, facilitating accurate discernment of tastants, especially with limited datasets. This will be discussed later.

To demonstrate the practical usefulness of this artificial bioinspired gustatory system, six commercial liquid food products, that is, orange juice, cola, pickled cucumber juice, seawater, white vinegar, and lemon juice, purchased from a local supermarket are analyzed with the hydrogel. The hydrogels are immersed in each liquid overnight to reach equilibrium, and then their resistance and volume variations are characterized. As depicted in Figure 4e, all liquids can be coarsely divided into three taste groups according to resistance response, that is, both the pickled cucumber juice and seawater show the greatest change in resistance like NaCl (0.17–1.71 M) regarded as saltiness; orange juice and cola as sweetness; white vinegar and lemon juice as sourness. The volume response falls in line with corresponding tastants (Figure 4b) and conforms with the resistance-change (Figure 4e), indicating the hydrogel's ability to identify different dominant tastes. For a further qualitative analysis in terms of complex commercial tastes, a machine learning model will be used and discussed later.

The artificial sweeteners have been widely used in various foods as substitutes for sugars.^[39] The improper use of sweeteners might cause adverse bioeffects ranging from liver toxicity to carcinogenicity.^[40,41] Thus, facile detection of sweeteners is of great practical impact. Notably, the present hydrogel responds differently to an artificial sweetener sodium cyclamate than to the natural sugar D(-)-fructose as both the volumetric and resistance

changes are distinct in Figure S11, Supporting Information, suggesting a qualitative, yet promising way to discern natural sugar and artificial sweetener.

2.3. Machine Learning

For a step further toward a more generic sensation, we introduce machine learning,^[42] intending for generic analysis of the tastants.^[43,44] The recent progress in machine learning has allowed, for example, image processing,^[45] tactile recognition,^[46] and neuromorphic computing.^[47] Here, a deep neural network (multilayer perceptron) is used to deal with both resistance and volume responses as the feature inputs, and nine outputs are defined, that is, weak, medium, and strong concentrations in sweetness, saltiness, and sourness (Figure 5a). The dataset is collected from Figure 4a,b. In our case, we define the concentration of salty NaCl tastants above 0.17 as high saltiness, between 0.17 and 0.086 M as the medium saltiness, and below 0.086 M as weak saltiness. Similarly, we define for both sweetness and sourness, the tastants' concentration is ≥ 0.086 as the weak taste, between 0.086 and 0.51 as the medium taste, and between 0.51 and 1.71 as the strong taste. Three hidden layers, each with 15, 25, and 20 nodes, are identified to precisely describe the relationship between the input and output data. In machine learning, the predictive accuracy increases significantly after ≈ 5 cycles of training which stabilizes thereafter (Figure S13, Supporting Information), indicating a training process. For the present limited dataset, it is a grand challenge to gain high accuracy. In our case, the accuracy is improved, and a lower prediction error is observed once both input signals of the resistance and the volume are used in contrast to when the resistance input signals are used only (Figures S13 and S14, Supporting Information). Consequently, the predicted concentrations are in concert with the actual concentrations of the resistance and volume signals collected from the hydrogels (Figure 5b), which is verified by the low errors between the prediction and reality (Figure 5c and Figure S12, Supporting Information), indicating a high accuracy in differentiating flavors.

Next, we analyze the signals from commercial beverages and foods (Figure 4e) based on this model. Surprisingly, the neural network not only recognizes all types of tastants and semi-quantifies the major tastant, but also identifies the mixed tastes in the product, for example, orange juice (Figure 4c). This signifies the further usage in discerning mixed tastant.

For mixed tastes, for example, sweetness and sourness, we again use a multilayer perceptron algorithm with three optimized hidden layers of 15, 25, and 15 nodes (Figure 5d). The concentration of each taste is graded into four categories, that is, weak, medium, strong, and super-strong concentrations, $\geq 0.086 \text{ M}$, 0.086 to 0.17 M, 0.17 to 0.51 M, and $\geq 0.51 \text{ M}$, respectively, in the complex mixed type. The neural network trained on the collected data (Figure 5e) can identify the concentrations of mixed sweetness and sourness in the solution with prediction probabilities higher than 58% (Figure 5f and Figure S15, Supporting Information). It increases the statistical reliability of detecting unknown tastes, even at mixed states.

Additionally, due to the hydrogel's temperature-insensitive characteristics in the detection of tastants (Figure S6b, Supporting Information) and the robustness of Deep Neural Networks

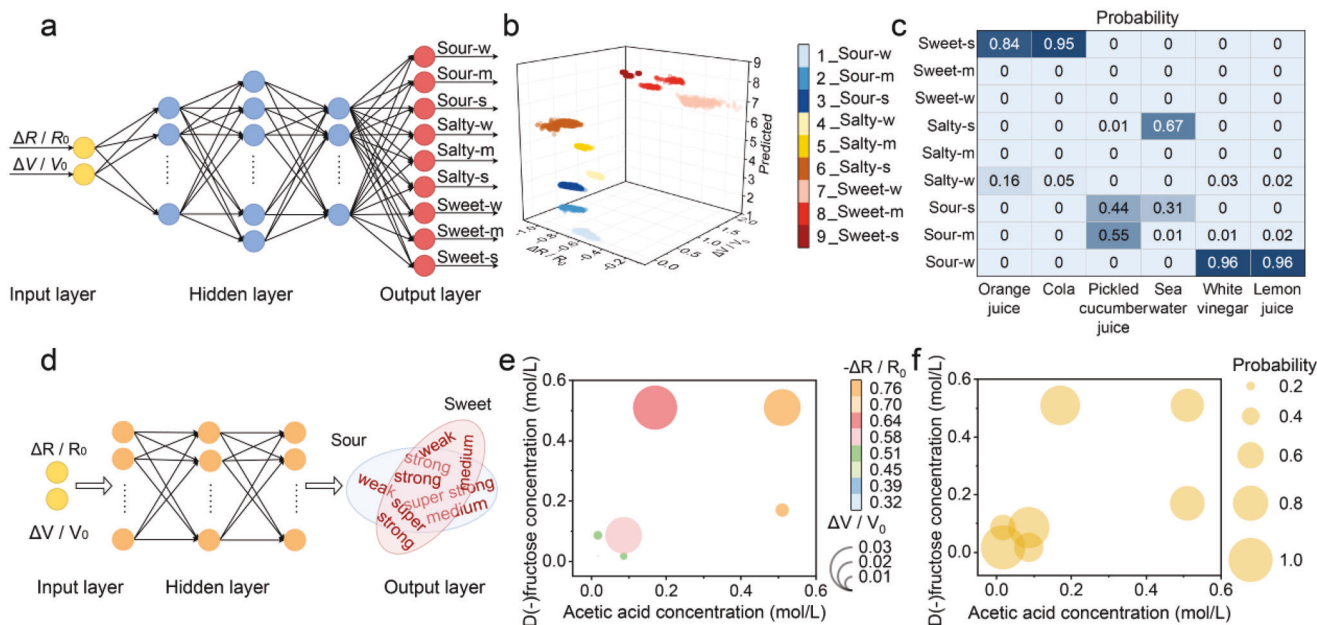


Figure 5. Machine learning-assisted taste recognition. a) Scheme of multilayer perceptron for three tastants. The “w,” “m,” and “s” refer to qualitative weak, medium, and strong levels of each flavor, respectively. b) Prediction graph – the axes show the relative resistance-change, relative volume-change, and corresponding predicted tastants. c) Predictions of samples in six beverages and food corresponding to different degrees of sweetness, sourness, or saltiness, obtained from the model with a multilayer perceptron. d) Scheme of multilayer perceptron for mixed tastes (sweetness and sourness). e) Resistance- and volume-response of hydrogels in mixed solutions of D(-)-fructose and acetic acid at different concentrations. f) Predictive accuracy of samples in mixed solutions – the axes show the D(-)-fructose concentration, acetic acid concentration, and corresponding predicted probability.

(DNNs) in handling slight variations, it can be inferred that the constructed model is resistant to minor temperature changes. We aim to investigate the impact of temperature in future research.

3. Conclusion

In summary, inspired by the bio-gustation system, a copolymeric hydrogel with tastant-responsiveness was developed by integrating nonionic HEMA and zwitter-ionic sulfobetainic DMAPS units into hydrogels. Varying the molar ratio between two units results in hydrogels with tunable optical, mechanical, and electrical properties. Markedly, the hydrogel responds to ionic and nonionic compounds differently, signaling electrical resistance and volume variations as the outcome. Taking both variations as the dual-input feature into machining learning allows for the semi-quantitative sensing of sweetness, saltiness, and sourness. It practically enables the identification of specific tastes in commercial foods and is further capable of the recognition of mixed tastes. This work suggests a promising strategy in the design of artificial tongues.

4. Experimental Section

Materials: [2-(Methacryloyloxy)ethyl] dimethyl-(3-sulfo)propyl ammonium hydroxide (DMAPS), 2-hydroxyethyl methacrylate (HEMA), *N,N,N',N'*-tetramethyl ethylenediamine, ammonium persulfate (APS), sodium chloride (NaCl), D(-)-fructose, acetic acid and sodium cyclamate were purchased from Sigma-Aldrich. All chemicals were analytical grade and were used as received. Ultrapure water obtained by Direct-Q 3 UV water purification system was used throughout experiments.

Preparation of Poly(DMAPS-co-HEMA) Hydrogels: Copolymer hydrogels were prepared by free-radical co-polymerization of DMAPS and HEMA monomers in deionized water. The molar ratios between HEMA and DMAPS varied from 75:25, 80:20, 86:14, 89:11, 91:0 to 100:0 with a fixed solid concentration of 30 wt%. The polymerization was proceeded with the initiator APS and the accelerator TEMED (both 0.2% of the total monomer molar ratio) in an oven at 70 °C for 6 h. Then, the hydrogel was washed five times with ultrapure water to remove unreacted chemical residues and further immersed in ultrapure water for 3 days to reach an equilibrium swelling ratio (Figure S16, Supporting Information).

Analytical Techniques: The focused ion beam-cut (FIB-cut) scanning electron microscopy (SEM) images of the hydrogel cross-section were acquired by a JEOL JIB-4700F FIB-SEM microscope. Fourier transform infrared (FTIR) spectra were recorded by PerkinElmer FTIR with Attenuated total reflection (ATR). Percent ultraviolet (UV) transmittance spectra were measured by a Cary 5000 UV-vis-NIR spectrophotometer with 5 mm-thickness hydrogels. Solid-state ¹³C nuclear magnetic resonance (NMR) was recorded by an Agilent 600 M spectrometer.

Mechanical Tests: The compression properties of poly(DMAPS-co-HEMA) hydrogels were measured by a mechanical testing apparatus (Instron 5567) at the uniaxial rate of 1 mm min⁻¹. The tunable hydrogel samples were prepared in cylindrical shapes with a diameter of 30 mm and a height of 10 mm. The tests ended when the compression reached 20% of the original height.

Electrical Measurements: Impedance data were measured with an Autolab electrochemical workstation (Metrohm Autolab PGSTAT302N potentiostat) at an alternating voltage of 0.1 V and a frequency sweep from 100 Hz to 1 MHz. Resistance signals were measured on a Keithley 2634B system source meter at a direct voltage of 1 V. All these characterizations were performed under normal ambient conditions.

The hydrogel was first cut into a cuboid, where the side length of the bottom square was ≈20 mm, and the height was ≈5 mm. It was sandwiched between two conductive thin copper plates, connected to conductive wires. The impedance data were analyzed using Nova 2.1 software, and the resistance values were obtained from the Nyquist plot. The ionic

conductivity σ of the hydrogel can be calculated according to the following formula:

$$\sigma = \frac{l}{RA} \quad (1)$$

where, l is the thickness of the hydrogel, R the electrical resistance of the hydrogel, A the contact area between hydrogel and copper plates.

Density Functional Theory Calculations: The interactions among DMAPS, HEMA, NaCl, acetic acid, D(-)fructose and their complexes were investigated using the Gaussian 16 package with DFT method^[48] at the ω B97XD/6-311G (d,p) level.^[49] The Bery geometries optimizations were carried out in vacuum and water, respectively, using the SMD solvent model.^[50] The harmonic frequency was calculated to verify there was no imaginary frequency. Then, the single-point energies of each system were calculated with the consideration of basis set superposition error (BSSE). All energies were corrected for zero-point vibrational energy.

The interaction energy of each system $E_{\text{interaction}}$ was calculated with the following equation:

$$E_{\text{interaction}} = E_{\text{AB}} - (E_{\text{A}} + E_{\text{B}}) + E_{\text{BSSE}} \quad (2)$$

where E_{A} and E_{B} represent the energies of A and B components, respectively. The E_{BSSE} is the BSSE corrected energy of each interaction pattern, and $E_{\text{interaction}}$ is the total energy required for binding A and B, where a negative value of $E_{\text{interaction}}$ indicates that the process is an exothermic reaction, hinting a stable product.

Artificial Neural Network: The classification network had an input layer with 2 input neurons, corresponding to inputs of the sensor resistance and volume, three hidden layers with 15, 25, and 20 neurons, respectively, as well as an output layer with 9 output neurons, corresponding to 9 tastes. The feature input was collected from 3 samples, with each sample consisting of 22 experimental datasets. Therefore, there is a total of 66 experimental datasets, each containing a value of resistance and a value of volume. To train the classification network, 11 000 datasets were generated (6600 for training, 2200 for validating, 2200 for testing) by adding 10% Gaussian noise to experimental dataset. The network was trained with a batch size of 21, epoch of 40. The test accuracy reaches 83.4% after training. Samples of mixed tastes were trained according to the same procedure, with three hidden layers (20 neurons in each layer).

Statistical Analysis: The software Microsoft Excel for Windows (Microsoft Office, 2020) was used for statistical calculations. All results were expressed as mean \pm standard deviation (SD), sample size $n = 3$, error bars correspond to SD.

Supporting Information

Supporting Information is available from the Wiley Online Library or from the author.

Acknowledgements

This work is supported by the Academy of Finland (No. 321443, 328942, 352671, 316973, and the Center of Excellence Program of Life-Inspired Hybrid Materials, project No. 346108), and the China Scholarship Council. This work acknowledges the facilities and technical support by Aalto University OtaNano-Nanomicroscopy Centre and Bioeconomy and Raw Materials Research Infrastructures.

Conflict of Interest

The authors declare no conflict of interest.

Data Availability Statement

The data that support the findings of this study are available from the corresponding author upon reasonable request.

Keywords

artificial tongues, bio-inspiration, gustation, hydrogel, machine learning, molecule sensing, taste

Received: June 22, 2023

Revised: September 13, 2023

Published online: October 6, 2023

- [1] G. J. Tortora, B. H. Derrickson, *Principles of Anatomy and Physiology*, John Wiley & Sons, Australia, **2018**.
- [2] D. A. Yarmolinsky, C. S. Zuker, N. J. P. Ryba, *Cell* **2009**, *139*, 234.
- [3] H. Lee, L. J. Macpherson, C. A. Parada, C. S. Zuker, N. J. P. Ryba, *Nature* **2017**, *548*, 330.
- [4] G. Q. Zhao, Y. Zhang, M. A. Hoon, J. Chandrashekar, I. Erlenbach, N. J. P. Ryba, C. S. Zuker, *Cell* **2003**, *115*, 255.
- [5] R. B. Chang, H. Waters, E. R. Liman, *Proc. Natl. Acad. Sci. USA* **2010**, *107*, 22320.
- [6] H. Garty, *FASEB J.* **1994**, *8*, 522.
- [7] S. D. Roper, N. Chaudhari, *Nat. Rev. Neurosci.* **2017**, *18*, 485.
- [8] M. Melis, I. T. Barbarossa, *Nutrients* **2017**, *9*, 541.
- [9] M. del Valle, *Electroanalysis* **2010**, *22*, 1539.
- [10] T. Wasilewski, W. Kamysz, J. Gębicki, *Biosens. Bioelectron.* **2020**, *150*, 111923.
- [11] N. A. Peppas, J. Z. Hilt, A. Khademhosseini, R. Langer, *Adv. Mater.* **2006**, *18*, 1345.
- [12] J. Kopeček, *Biomaterials* **2007**, *28*, 5185.
- [13] A. Khan, S. Ahmed, B.-Y. Sun, Y.-C. Chen, W.-T. Chuang, Y.-H. Chan, D. Gupta, P.-W. Wu, H.-C. Lin, *Biosens. Bioelectron.* **2022**, *198*, 113811.
- [14] J. Yeom, A. Choe, S. Lim, Y. Lee, S. Na, H. Ko, *Sci. Adv.* **2020**, *6*, eaba5785.
- [15] L. Yang, Z. Wang, S. Zhang, Y. Li, C. Jiang, L. Sun, W. Xu, *Nano Lett.* **2022**, *23*, 8.
- [16] J. Liu, Y. K. Cha, Y. Choi, S.-E. Lee, G. Wang, S. Zhao, T. H. Park, Y. Liu, S. Hong, *ACS Sens.* **2023**, *8*, 2750.
- [17] R. V. Kulkarni, S. A. Biswanath, *J. Appl. Biomater. Biomech.* **2007**, *5*, 125.
- [18] Y. Lee, W. J. Song, J.-Y. Sun, *Mater. Today Phys.* **2020**, *15*, 100258.
- [19] W. Geurtsen, *Crit. Rev. Oral Biol. Med.* **2000**, *11*, 333.
- [20] J.-P. Montheard, M. Chatzopoulos, D. Chappard, *J. Macromol. Sci., Part C* **1992**, *32*, 1.
- [21] X. Lou, S. Vijayasekaran, T. V. Chirila, M. A. L. Maley, C. R. Hicks, I. J. Constable, *J. Biomed. Mater. Res.* **1999**, *47*, 404.
- [22] X. Lou, P. D. Dalton, T. V. Chirila, *J. Mater. Sci. Mater. Med.* **2000**, *11*, 319.
- [23] N. Nishiyama, K. Suzuki, K. Komatsu, S. Yasuda, K. Nemoto, *J. Dent. Res.* **2002**, *81*, 469.
- [24] A. Dixit, D. S. Bag, S. J. S. Kalra, *Polymer (Guildf)* **2017**, *119*, 263.
- [25] Q. Shao, S. Jiang, *Adv. Mater.* **2015**, *27*, 15.
- [26] P. Liu, J. Song, *Biomaterials* **2013**, *34*, 2442.
- [27] A. Eklund, H. Zhang, H. Zeng, A. Priimagi, O. Ikkala, *Adv. Funct. Mater.* **2020**, *30*, 2000754.
- [28] D. S. Wiersma, *Nat. Photonics* **2013**, *7*, 188.
- [29] J. H. Gouda, K. Povodator, T. C. Warren, W. Prins, *J. Polym. Sci., Part B: Polym. Phys.* **1970**, *8*, 225.
- [30] J. Nan, G. Zhang, T. Zhu, Z. Wang, L. Wang, H. Wang, F. Chu, C. Wang, C. Tang, *Adv. Sci.* **2020**, *7*, 2000587.
- [31] X. Zhang, B. Wu, S. Sun, P. Wu, *Adv. Funct. Mater.* **2020**, *30*, 1910425.
- [32] A. Allagui, T. J. Freeborn, A. S. Elwakil, B. J. Maundy, *Sci. Rep.* **2016**, *6*, 38568.
- [33] F. Wang, J. Yang, J. Zhao, *Polym. Int.* **2015**, *64*, 999.
- [34] K. Nakamura, *Polym. J.* **1976**, *8*, 267.

- [35] B. P. Halpern, *Neurosci. Biobehav. Rev.* **1986**, *10*, 135.
- [36] X. Liu, J. Liu, S. Lin, X. Zhao, *Mater. Today* **2020**, *36*, 102.
- [37] R. N. Goldberg, N. Kishore, R. M. Lennen, *J. Phys. Chem. Ref. Data* **2002**, *31*, 231.
- [38] B. Lindemann, *Physiol. Rev.* **1996**, *76*, 719.
- [39] S. Kojima, H. Ichibagase, *Chem. Pharm. Bull. (Tokyo)* **1966**, *14*, 971.
- [40] F. E. Ahmed, D. B. Thomas, *Crit. Rev. Toxicol.* **1992**, *22*, 81.
- [41] S. Takayama, A. G. Renwick, S. L. Johansson, U. P. Thorgeirsson, M. Tsutsumi, D. W. Dalgard, S. M. Sieber, *Toxicol. Sci.* **2000**, *53*, 33.
- [42] J. Schmidhuber, *Neural Networks* **2015**, *61*, 85.
- [43] J.-H. Kim, *Comput. Stat. Data Anal.* **2009**, *53*, 3735.
- [44] C.-C. Chang, C.-J. Lin, *ACM Trans. Intell. Syst. Technol.* **2011**, *2*, 1.
- [45] M. Wu, L. Chen, in *2015 Chinese Automation Congress (CAC)*, IEEE, **2015**.
- [46] H. Tan, Q. Tao, I. Pande, S. Majumdar, F. Liu, Y. Zhou, P. O. Å. Persson, J. Rosen, S. van Dijken, *Nat. Commun.* **2020**, *11*, 1369.
- [47] K. Roy, A. Jaiswal, P. Panda, *Nature* **2019**, *575*, 607.
- [48] W. Kohn, L. J. Sham, *Phys. Rev.* **1965**, *140*, A1133.
- [49] J.-D. Chai, M. Head-Gordon, *J. Chem. Phys.* **2008**, *128*, 84106.
- [50] A. V. Marenich, C. J. Cramer, D. G. Truhlar, *J. Phys. Chem. B* **2009**, *113*, 6378.